



Jet-induced skin puncture and its impact on needle-free jet injections: Experimental studies and a predictive model

Joy Baxter¹, Samir Mitragotri^{*}

Department of Chemical Engineering, University of California, Santa Barbara, CA 93106, United States

Received 2 November 2004; accepted 12 May 2005
Available online 5 July 2005

Abstract

Needle-free jet injections constitute an important method of drug delivery, especially for insulin and vaccines. This report addresses the mechanisms of interactions of liquid jets with skin. Liquid jets first puncture the skin to form a hole through which the fluid is deposited into skin. Experimental studies showed that the depth of the hole significantly affects drug delivery by jet injections. At a constant jet exit velocity and nozzle diameter, the hole depth increased with increasing jet volume up to an asymptotic value and decreased with increasing values of skin's uniaxial Young's modulus. A theoretical model was developed to predict the hole depth as a function of jet and skin properties. A simplified model was first verified with polyacrylamide gels, a soft material in which the fluid mechanics during hole formation is well understood. Prediction of the hole depth in the skin is a first step in quantitatively predicting drug delivery by jet injection.

© 2005 Elsevier B.V. All rights reserved.

Keywords: Jet injection; Skin; Hole depth; Dead-end channel; Polyacrylamide gels; Turbulent jet theory; Young's modulus; Critical stress

1. Introduction

Jet injection is an important needle-free drug delivery method for administration of insulin, human growth hormone, and vaccines [1,2]. Jet injections employ a high-speed jet to puncture the skin and deliver drugs without the use of a needle. Although jet injections have been used for the past 60 years [1]

and continue to be researched for new applications [3,4] studies on their mechanism are emerging only now [5–7]. These studies have suggested that a high-speed jet forms a hole in the skin early in the injection and subsequently disperses the fluid through the hole into the porous skin structure [6].

Formation of a hole is a first critical step in needle-free liquid jet injections. While previous reports have documented the existence of a jet-induced hole [8], little work has been done to quantify or predict the dimensions of the hole created in the skin. Reports have suggested that the width of the hole is on the order of the diameter of the jet (~100 μm), smaller than the diameter of standard needles (0.41–0.71 mm) and that jet-

^{*} Corresponding author. Tel.: +1 805 893 7532; fax: +1 805 893 4731.

E-mail address: samir@engineering.ucsb.edu (S. Mitragotri).

¹ Current address: Unilever Research and Development, 40 Merriitt Blvd., Trumbull, CT. 06611.

induced holes in the skin heal in the same amount of time as holes due to needle insertion (24–48 h) [9]. However, no information exists on the depth of the hole in the skin. The depth of the hole is a critical factor in determining the depth of fluid penetration after jet injections. Accordingly, an in-depth understanding of the factors that influence the hole depth and a predictive model to describe the hole depth are necessary to reliably administer drugs intradermally, subcutaneously, or intramuscularly. Furthermore, such understanding may also aid in avoiding interactions with nerve endings suggested to be the primary source of pain associated with jet injections.

The objective of this study is to understand jet-induced puncture of skin using experimental and theoretical studies with emphasis on assessing the dependence of hole depth on skin's mechanical properties. Prediction of the hole depth in the skin requires the development of a model that incorporates the fluid dynamics of the jet as well as a mechanical property of skin that dictates skin failure. Since the fluid dynamics of polyacrylamide gels is less complex compared to skin, the model was first tested in gels. Polyacrylamide gels have been used as a model test bed for several fluid impingement applications [10,11]. They meet several criteria for a model soft material including transparency, controllable mechanical properties, and controllable dimensions. Models describing jet-material interactions have been previously reported for soil erosion as well as for abrasive jet cutting [12,13]. However, interactions of materials with abrasive jets are fundamentally different than those with plain water jets, thus limiting the applicability of these theories to describe jet injections into skin [12,13]. Theories for erosion of soil and non-cohesive particulate materials by circular turbulent liquid jets have been developed but are not applicable to skin since they are based on semi-empirical equations or require information about the particle size of the material, a parameter that is clearly non-relevant for skin [14,15].

2. Materials and methods

2.1. Jet production

The jets used in this study were produced using a commercial, spring-driven jet injector, Vitajet 3 (Bio-

ject Inc.; Portland, OR, USA) through orifices of 76 to 304.8 μm in diameter. Jet velocities ranged from 110 to 200 m/s, determined using the jet ejection period which was measured with a piezoelectric transducer (Dynasen, Inc., Goleta, CA, USA) [5]. Jets were ejected under submerged conditions at standoff distances between 1 and 5.8 mm from the skin or gel maintained using a spacing ring. Submerged conditions were created by placing the jet fluid inside the spacing ring, inner diameter of 5.6 mm, prior to injection. The ring was sealed to the skin or gel with vacuum grease. The jet fluid was either a solution of sulforhodamine B [1.5 mM] or ^3H labeled mannitol [10 $\mu\text{Ci/ml}$] in deionized (DI) water [5,7].

2.2. Measurement of drug delivery into skin

Human and porcine skin was used in the jet penetration experiments. Human skin (abdominal) was procured through the National Disease Research Interchange and was frozen at $-70\text{ }^\circ\text{C}$ until the time of experiments. Skin was procured from three Caucasian males ages 53, 54, and 64 and one Caucasian female, age 57. Porcine skin was harvested from Yorkshire pigs (ages 3–4 months) and was excised from around the torso immediately after sacrificing the animal. The full thickness skin was cleaned to remove fat and subdermal tissues, and was frozen to $-70\text{ }^\circ\text{C}$ until the time of experiments. All experiments were performed according to institutionally approved protocols.

Jet penetration into skin was quantified using radiolabeled mannitol and jet dispersion was assessed using a colorimetric dye sulforhodamine B (SRB). For each type of experiment, skin, supported by a wire mesh, was placed on a Franz diffusion cell (FDC, PermeGear, Hellertown, PA, USA). The receiver compartment of the FDC was filled with phosphate buffered saline (phosphate concentration of 0.01 M and NaCl concentration of 0.137 M, pH=7.4 at $25\text{ }^\circ\text{C}$). Each piece of skin was taped on all sides to prevent any fluid leakage. This experimental setup was previously validated to represent *in vivo* jet injections [5].

2.3. Measurement of hole depth in skin

The depth of the hole was measured using the “wire technique” in which a 36-gauge copper wire (127 μm in diameter) was inserted into the hole in the skin

created by the jet (Fig. 1a). The wire was inserted in the hole in skin post injection with the aid of a stereo microscope. A flag was placed on the wire to mark a set distance. The hole depth was calculated by subtracting the distance from the flag to the surface of the skin from the distance from the flag to the end of the wire, as measured using digital imaging. The insertion of the wire did not cause additional skin failure even after multiple insertions. Repeated measurements ($n=3-4$) of each hole yielded a typical standard deviation of 200 μm . The wire technique can be performed quickly and immediately after the injection but is limited in application by the finite diameter of the wire. This wire technique was validated, when possible, by visual confirmation of the hole depth after cross-sectioning the skin with a razor blade (data not shown). The error associated with the wire technique is thought to originate from the tapering of the hole at the distant end; however, the exact value of the error is not known. The wire measurement method was found to be more reliable than methods based on direct visualization. Direct observation of the hole after cross-sectioning the skin with a razor blade did not clearly show the contrast between the hole and the unperturbed skin. Another direct visualization technique to determine hole depth as well as hole width is to section the skin using a microtome. This process is time consuming and limits the number of experiments performed. In addition, it is difficult to visualize tortuous holes necessitating, for example, as many as 80 consecutive sections for a hole 200 μm in width to determine the hole depth.

2.4. Measurement of mechanical properties of skin

Uniaxial tension tests were performed on human and porcine skin in vitro to determine the uniaxial Young's modulus. The skin was prepared for testing by cutting full thickness skin in strips of 2.5 cm in width and 8 to 13 cm in length. The testing was performed with the skin in air using a universal mechanical tester (Instron 1123, Canton, MA, USA) at a cross-head speed of 1.27 cm/min and using a 22 000 N (5000 lb) tension load cell. The stress on the skin (σ) was determined by measuring the force on the sample (F) and dividing it by the original cross-sectional area of the sample (A_{oc}) (Eq. (1)).

$$\sigma = \frac{F}{A_{oc}} \quad (1)$$

A laser extensometer (Electric Instrument Research, Irwin, PA, USA) was used to measure the strain of the skin (ε). The initial length and the elongation of the skin were measured by the laser extensometer. The strain was calculated by dividing the elongation by the initial length. The stress-strain curve is non-linear for skin. The Young's modulus of skin (E_{skin}) was therefore determined from the initial slope of the stress-strain curve (Fig. 2, Eq. (2)).

$$E_{\text{skin}} = \left[\frac{d\sigma}{d\varepsilon} \right]_o \quad (2)$$

The average Young's modulus, calculated from the initial slope, was based on 4–8 measurements.

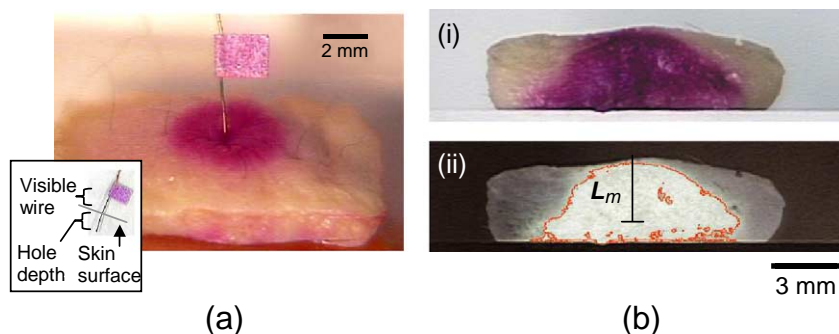


Fig. 1. (a) A wire technique was developed to measure the hole depth in skin. A wire was inserted in the hole in human skin after jet injection of a dyed solution (hole not visible in the picture). The inset depicts that the hole depth was calculated by visualizing the exposed part of the wire. (b) (i) The dispersion of fluid is visible by cross-sectioning the skin after injection of a dyed solution. (ii) The dispersion is quantified by the parameter L_m , the distance from the top of the skin to the maximum width of dispersion, measured after image processing [7].

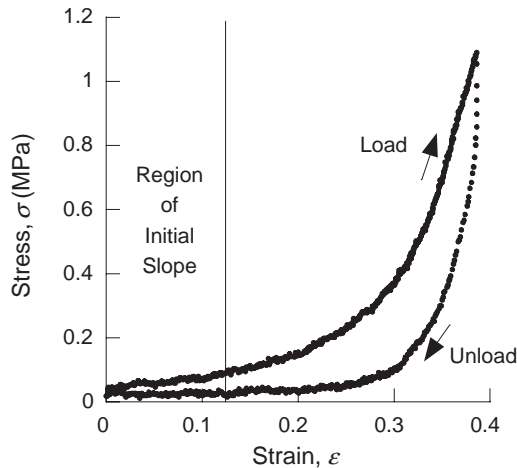


Fig. 2. A representative stress–strain curve for human skin. Note the hysteresis in the curve. Young's modulus was determined from the initial slope of the curve (strain less than 0.2).

2.5. Rate of hole formation in skin

High-speed photography was utilized to determine the failure rate of the skin. Skin (porcine abdominal) was thinned mechanically using wet/dry sand paper (3 M wet or dry tri-m-ite 80) on the underside of the

dermis. The skin was terraced to five different thicknesses from 0.3 to 1.6 mm. Jet injections were performed on the thinned skin areas and the jet was visualized as it impacted the top of the skin and later penetrated through the skin (Fig. 3b). The experimental setup was similar to that used in needle penetration experiments in literature (Fig. 3a) [16]. The skin was secured to a wood dowel using a thread and kept taught with a weight which had a mass of 132 g. A Kodak Ektapro 4500 motion analyzer was used to capture the jet crossing the entire skin thickness at 18,000 frames per second. The failure rate was determined from the time required for penetration of a 122 m/s jet (nozzle diameter of 229 μm ejected above the skin about 2.5 mm, unsubmerged) through the different thicknesses of skin.

2.6. Polyacrylamide gels

Polyacrylamide gels (10–30% acrylamide) were used as model soft materials. The gels were created by the addition of initiators (10% ammonium persulfate (APS) and *N,N,N',N'*-tetramethylethylenediamine (TEMED)) to a 40% (w/v) acrylamide solution (Bio-Rad Laboratories, Hercules, CA, USA). Acryl-

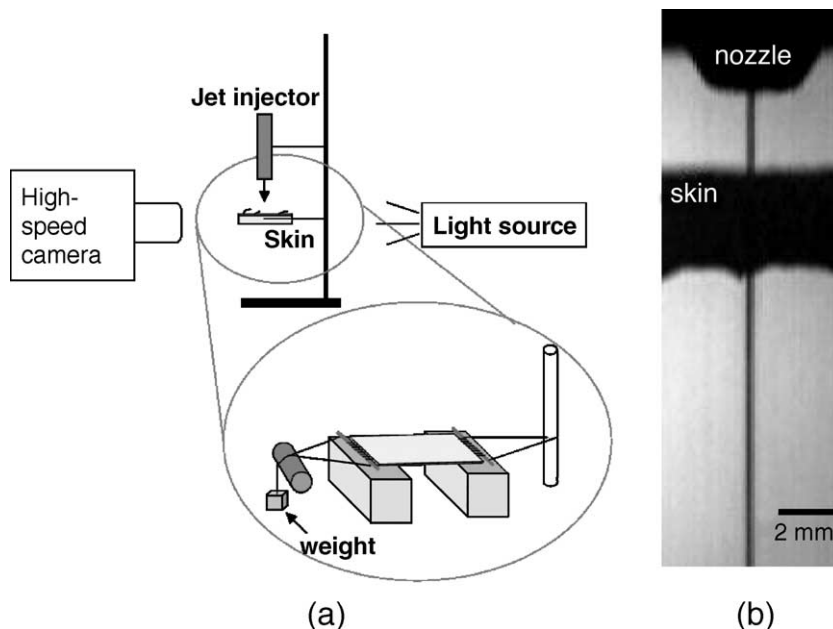


Fig. 3. (a) Experimental setup used for determining the rate of hole formation during jet penetration through human skin. (b) Image from a single frame showing jet penetration through skin. The actual thickness of the skin is smaller than that seen due to curling on the edges.

amide solution (40% w/v) was mixed with DI water to create solutions possessing various acrylamide concentrations in the range of 10% to 30% w/v. Gels were polymerized by the addition of 10% APS and TEMED to 6 ml acrylamide solution. The volumes of APS solution used for polymerization were 30, 34, 60, 38, and 45 μl for 10%, 15%, 20%, 25% and 30% gels, respectively. The volumes of TEMED solution used for polymerization were 6, 9, 12, 10, and 12 μl for 10%, 15%, 20%, 25% and 30% gels, respectively.

2.7. Measurement of mechanical properties of gels

The compressive failure stress and the shear failure stress of the gels were measured using a universal mechanical tester (Instron 1123, Canton, MA). Compressive failure testing was performed in air using an 890 N (200 lb) compression load cell. Gels were compressed with a cross-head speed of 0.127 cm/min until failure at which time the gel broke into many pieces. Each gel piece was cylindrical in shape, approximately 13 mm in diameter and 20 mm in height. The diameter of the cross-head was 5 cm. To measure shear failure stress, the cylindrical gels were placed horizontally within two metal blocks 1 mm apart with cylindrical holes slightly bigger than the gel. One metal block was held steady and the other moved vertically at 0.127 cm/min until the gel fractured under shear. The force was measured with an 890 N (200 lb) tension load cell. The fracture surfaces were examined after testing. The experiments in which fracture surface was not near 90° from the cylindrical walls were eliminated.

3. Theory

3.1. Basic premise of the theory

It was assumed that the stress due to jet impingement on the material is responsible for the material failure in the direction of the jet. The critical stress for failure due to jet impingement, σ_c , can then be defined using Bernoulli's equation:

$$\sigma_c = \frac{1}{2} \rho u_{mc}^2 \quad (3)$$

where u_{mc} is the critical centerline velocity required to induce failure and ρ is the density of the jet fluid. σ_c can be experimentally measured for polyacrylamide gels but a method to directly measure the same for skin is not obvious. Several different types of skin failure parameters have been previously measured. The work of fracture of human skin, which is the work required to propagate a crack, has been determined by two different methods: a scissors cutting test and microneedle insertion [17,18]. In addition, the critical stress for failure under uniaxial tension of porcine skin was determined to be about 15 MPa [19]. However, it is unclear whether these parameters effectively represent σ_c for skin. Accordingly, σ_c for skin needs to be determined indirectly. For this purpose, fluid dynamic equations were used to predict u_m as a function of depth. These equations, along with Eq. (3), were fitted to experimentally measured hole depths to determine u_{mc} and hence σ_c for skin.

3.2. Dependence of hole depth on time and jet volume

Experimental data showed that the depth of the holes created in the skin and gel increases with time during the injection [6] and ejected volume (Fig. 4) before reaching an asymptotic value (typically beyond a jet volume of 0.13 ml). This means that once the asymptotic hole depth is reached the critical stress for skin failure is no longer met and the resulting asymptotic value represents a steady-state geometry. The existence of asymptotic hole depths has been documented for other processes such as the erosion of soil [20]. Since the asymptotic hole depths are independent of time and jet volume, they represent a material property and hence are compatible with Eq. (3) which is also independent of time and jet volume. In addition, the choice of the asymptotic hole depth as the output parameter of the model eliminated the need to understand the microscopic failure modes (erosion, cutting, or crack formation) through which the hole is formed. It is interesting to note that the hole depth is a nonlinear function of volume (Fig. 4) while a linear function of time [6]. Further investigations are required to resolve this peculiarity. Experimentally measured and theoretically predicted hole depths referred to hereafter represent the asymptotic limits.

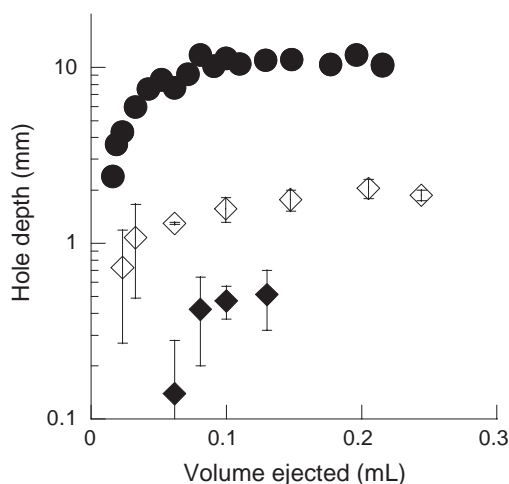


Fig. 4. The hole depths created in human skin (\diamond), porcine skin (\blacklozenge), and polyacrylamide gel (20% acrylamide, \bullet) were dependent on the volume of fluid ejected from the injector. As the ejected volume increased, the hole depths in each material approached an asymptotic value which was dependent on the material as well as the experimental jet conditions. Experimental hole depths throughout this document are reported at their asymptotic limit. Practically, an ejection volume of 0.13 ml was used at which the values of the hole depths were very close to their asymptotic limit.

3.3. Differences in hole formation in gels and skin

To utilize Eq. (3) it is necessary to describe the centerline velocity of the jet in the hole. The overall goal of the model is to describe the asymptotic hole depths. In other words, the goal of the model is to describe the steady-state hole depth using the fluid dynamics of the jet during hole formation. The centerline velocity of the jet during hole formation is dependent on the geometry and dimensions of the hole, determined in part by the rate at which the hole is formed. The volumetric rate of failure of skin (abdominal porcine), as assessed by high-speed photography, was determined to be $0.1 \text{ cm}^3/\text{s}$ which was nearly fifty times lower than the experimental volumetric flow rate of the jet, $5.0 \text{ cm}^3/\text{s}$. Hence, there exists a significant backflow of the jet during hole formation in the skin (depicted schematically in Fig. 5). Fluid undergoing backflow from the hole slows down the fluid entering the hole and decreases the ability of the jet to cause further failure of the skin. The presence of backflow in the hole significantly complicates the fluid dynamics. In contrast, the rates of failure of polyacrylamide gels were

comparable to the volumetric flow rate out of the injector [6]. Therefore, there is no apparent backflow in the hole created in polyacrylamide gels (Fig. 5). Hence, the centerline velocity of the jet during hole formation in polyacrylamide gels and the resulting hole depth can be described by relatively simpler equations. Due to differences in jet behavior in polyacrylamide gels and skin, two separate models were developed to predict hole depths in the two materials.

The jets used throughout the experimental studies in this manuscript were circular, submerged, and turbulent in nature with Reynolds numbers from 7600 to 40000. Fluid dynamics of circular submerged turbulent jets has been well studied both theoretically and experimentally [21–23]. A jet is “submerged” when the jet and surrounding fluid are the same, such as a water jet in water or an air jet in air. The structure of a turbulent jet consists of two significant regions: initial region (developing flow) and main region (developed flow) (Fig. 6a). The initial region is defined by the presence of a jet core in which the fluid travels at the exit velocity, u_0 . Once the centerline velocity, u_m , is no longer equal to u_0 the initial region ends and the main region begins. In the experimental system a water jet travels in a pool of water for a standoff distance, x_s , before it encounters the interface with the skin or polyacrylamide gel. The structure as well

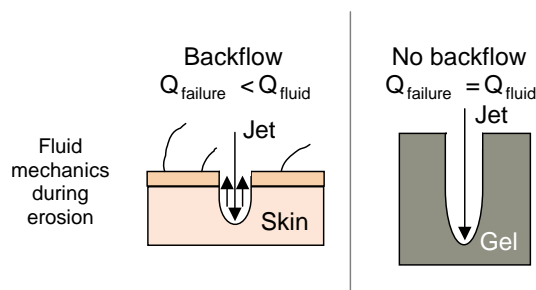


Fig. 5. The fluid mechanics during hole formation in skin and polyacrylamide gels is depicted in this cartoon (image not to scale). The critical difference between the two systems is the presence of fluid backflow in the skin but not in polyacrylamide gels. The presence of backflow was determined by examining the volumetric rate of failure, Q_{failure} , in both skin and polyacrylamide gels and comparing it to the volumetric flow rate of the jet, Q_{fluid} . Q_{failure} of abdominal porcine skin was determined by motion analysis to be nearly fifty times slower than Q_{fluid} . However, Q_{failure} for polyacrylamide gels was nearly the same as Q_{fluid} .

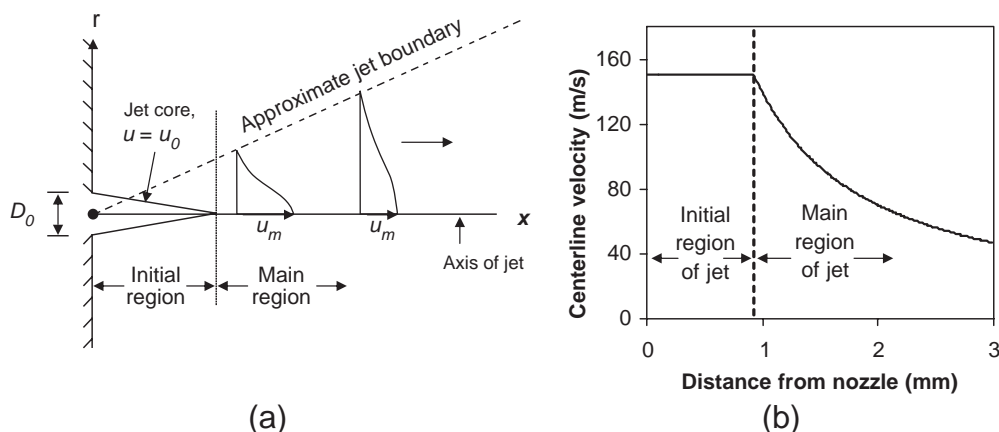


Fig. 6. (a) The structure of a submerged turbulent jet in an infinite solution is known to consist of an initial region containing the jet core ($u_m = u_0$) and a main region of flow in which the jet is fully developed (image not drawn to scale). As the distance from the nozzle exit increases the centerline velocity of the jet, u_m , decreases. This is depicted in panel (b) using Eq. (4) for the main region of the jet with initial conditions of $u_0 = 150$ m/s and $D_0 = 152$ μm .

as the spatial velocity vectors of a submerged jet are well understood due to theoretical assumptions that are applicable for this submerged system [21–23], as opposed to a water jet ejected into air [24].

3.4. Fluid dynamics of jets with no backflow

Since there is no appreciable backflow of fluid during jet penetration into polyacrylamide gels, we assumed that the centerline velocity in the gel system could be described by that of a “free jet” (a submerged jet traveling in an infinite stagnant fluid). In doing so, it was assumed that the side walls of the hole have a negligible effect on the centerline velocity. It was also assumed that the centerline velocity immediately preceding the impingement region is the appropriate velocity to use in Eq. (3) and that this velocity can be approximated using Eq. (4) when x is equal to the distance of the end of the hole from the nozzle orifice. The centerline velocity in the main region (Fig. 6a) of a free jet varies with distance, x , as follows assuming constant momentum in the axial direction [22,23] (Fig. 6b):

$$u_m = \frac{1}{2C_2} \frac{u_0 D_0}{x}, \quad (4)$$

where D_0 is the nozzle diameter. C_2 is an experimentally determined constant characterizing the spreading of the jet and has been reported to be 0.081 [22]. The

length of the initial region, x_0 , is derived from Eq. (4) by substituting u_m for u_0 .

$$x_0 = \frac{D_0}{2C_2} \quad (5)$$

The simplified model for the magnitude of the hole depth, h_d , due to an impinging jet was derived by substituting Eq. (5) into Eq. (3) when x is replaced by $h_d + x_s$ as follows:

$$h_d = \frac{u_0 D_0}{2C_2} \sqrt{\frac{\rho}{2\sigma_c}} - x_s. \quad (6)$$

3.5. Fluid dynamics of jets with backflow

The fluid dynamics of a turbulent jet in a dead-end channel (with backflow) has been studied experimentally and theoretically for incompressible fluids [21,25]. A theoretical analysis is presented in Chapter 10 of *The Theory of Turbulent Jets* [21]. The equations developed in this reference do not adequately describe experimental data presented therein or additional literature data [25] necessitating the development of more appropriate equations as presented here. Like flow under no backflow conditions, flow in a dead-end channel exhibits a decrease in centerline velocity with distance. However, the shape of the decay is different. The decrease in the non-dimensional centerline velocity (u_m/u_0) with increasing non-

dimensional distance (x/D_0) is essentially linear as determined from data in Ref. [25]. This dependence was approximated by a linear relationship ($r^2=0.96-0.99$):

$$\frac{u_m}{u_0} = m \left(\frac{x}{D_0} \right) + b, \quad (7)$$

where b is a constant. The average value of b determined from the data in Ref. [25] was 1.1 with a standard deviation of 0.02. The slope, m , depends on α , the ratio of D_0 to the hole diameter, H , ($\alpha=D_0/H$) as determined from Fig. 8 in Ref. [25] (Eq. (8); $r^2=0.99$, $n=3$).

$$m = -0.25\alpha - 0.02 \quad (8)$$

The precise value of α can only be obtained after determining hole diameter, H . This was done for polyacrylamide gels and α was found to be 0.3. As a first approximation, it was assumed that the same value of α can be used for skin as well. This approximation should be revisited once accurate measurements of the hole diameter are obtained for skin. Eqs. (7) and (8) were combined to describe the centerline velocity in a dead-end channel.

$$u_m = u_0 \left(1.1 - (0.25\alpha + 0.02) \frac{x}{D_0} \right) \quad (9)$$

Eq. (9) is an empirical equation for the centerline velocity in a dead-end channel that is sufficiently long to allow the flow to develop. The centerline velocity in Eq. (9) should be considered approximate especially when applied to the skin system which typically has a relatively short hole. Further experimental and theoretical work on flow in dead-end channels would strengthen the representation of the centerline velocity (Eq. (9)) and bring to light knowledge on this complex system.

The hole depth in the skin is described by Eq. (10) in which Eqs. (3) and (9) were combined when x is replaced by h_d as follows:

$$h_d = \frac{D_0}{(0.25\alpha + 0.02)} \left[1.1 - \frac{1}{u_0} \sqrt{\frac{2\sigma_c}{\rho}} \right]. \quad (10)$$

Eq. (10) relates the hole depth to the critical stress of skin failure, the density of the fluid, and the jet properties of exit velocity and nozzle diameter. However, the standoff distance does not appear in this equation. It is unclear how the centerline velocity in

the hole would be affected by the introduction of a standoff distance without additional fluid dynamics data. Therefore, hole depths at various standoff distances cannot be predicted by this model. It has been assumed that the experimental hole depths in skin, which have been measured for a submerged system with a standoff distance of 1 mm, can be predicted using Eq. (10). This assumption does not affect the validity of the equations but may affect the values of σ_c since it is fitted to the data. Eq. (10) is valid when Eq. (7) produces positive values of u_m .

4. Results and discussion

4.1. Hole formation–dispersion mechanism of jet injection

Prior to applying the theory to experimental data, it was deemed necessary to verify that jet penetration into skin indeed occurs by skin puncture followed by jet dispersion. The existence of such a mechanism was previously proposed based on dynamic visualization of interactions between the jet and the polyacrylamide gels [6]. Investigations of the location of fluid deposited in skin by jet injection gave further evidence of this mechanism. The dispersed fluid under different conditions resembled subsections of spheres [7]. That is, the outline of the fluid when deposited primarily in the skin has been found to have the shape of an upper hemisphere, a spheroid, or a lower hemisphere suggesting that these shapes were a result of a point-source flow from the center of the spheres [7]. In this study, experimentally measured hole depths were compared to the parameter L_m , defined as the distance from the top of the skin to the maximum width of dispersion (Fig. 1b) as determined by visualization of jet dispersion in the skin [7]. The hole depths coincided with L_m , which represents the center of a spherical dispersion, through the ~ 3 mm maximum thickness of the skin (Fig. 7). The hole depths varied from 0 to 2.71 mm as L_m increased from 0.05 to 2.43 mm. This range of h_d was created by injecting fluid into skin samples (human and porcine) from different anatomical sites possessing varying mechanical properties with jets of various parameters. The linear correlation ($r=0.96$) between h_d and L_m confirms that drug delivery by jet injection occurs first by

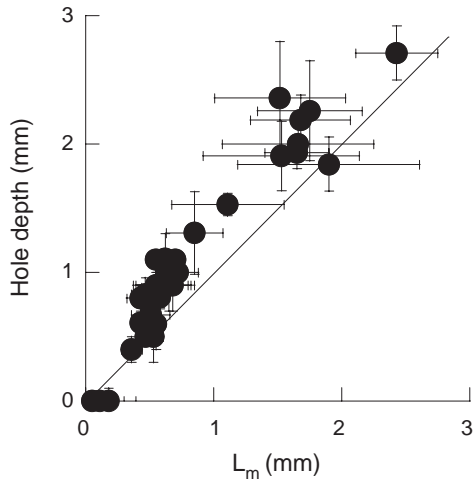


Fig. 7. The hole depth measured in skin correlates nearly 1:1 with the parameter L_m measured from the fluid dispersion confirming the hole formation–dispersion mechanism. The range of hole depths were created by injecting different skin samples under various jet conditions ($n=3-5$).

creation of a hole of depth $\sim L_m$ followed by dispersion originating at L_m . Since the majority of dispersion occurs at a depth h_d in the skin, it can be ascertained that hole formation occurs early in the injection. This conclusion appears to be valid regardless of the jet or skin properties over the range tested in this study. The correlation between the h_d and L_m also allows easy detection of the hole depth simply by injecting skin in vitro with a dyed fluid and observing the cross-section. Furthermore, from previous knowledge on the dependence of L_m on jet properties [7] the dependence of hole depth on jet properties can be deduced.

4.2. Dependence of jet injections on skin’s mechanical properties

The mechanical properties of skin have a direct influence on drug delivery by jet injection. Several mechanical properties of skin including Young’s modulus, critical stress for failure, fracture toughness, and hardness may play important roles in determining jet penetration. As a first step, the dependence of hole depth and fluid delivery on skin’s uniaxial Young’s modulus, E_{skin} was investigated. The Young’s modulus which is a measure of the elasticity of the skin may be an indicator of the internal structure such as the

density of collagen fibers which may affect both jet penetration and dispersion within skin. The average Young’s modulus of the human abdominal skin pieces used in this study was 0.3 MPa (± 0.09 MPa). Porcine skin pieces possessed Young’s moduli ranging from 0.5 MPa for abdominal skin to 1.0 MPa for dorsal skin. The Young’s modulus of porcine skin is highly dependent on the anatomical location of the skin. Abdominal porcine skin most closely modeled human skin as assessed by the Young’s modulus, quantitative delivery, and hole depth. By using porcine as well as human skin, it was possible to assess the influence of skin’s properties on the hole depth over a wide range of E_{skin} . Both the hole depth and the fluid delivery decreased with increasing Young’s modulus (Fig. 8). As the hole depth increased from 0.6 to 1.7 mm the percent delivery increased from 6% to 100% (of ejected liquid). The variation in jet delivery due to E_{skin} may partially (if not completely) explain the necessity of person-to-person optimization of injector settings which is recommended by most jet injector manufacturers. Skin thickness has also been shown to be a factor in determining variations in delivery for subcutaneous

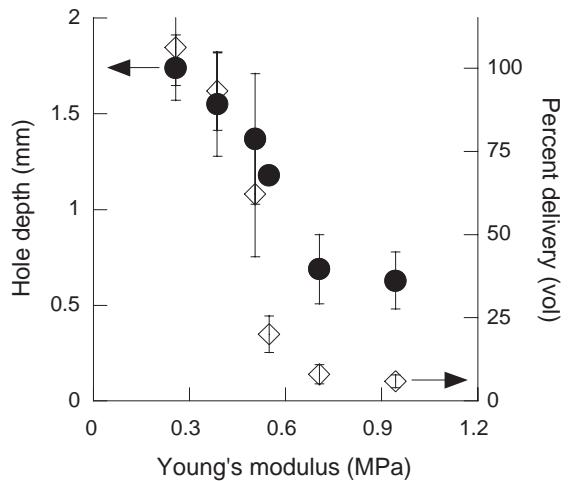


Fig. 8. The Young’s modulus of skin plays an important role in controlling the hole formation in the skin and the amount of fluid delivered to the skin. As the Young’s modulus increases the hole depth (closed circle) as well as the percent of fluid delivered to the skin (open diamonds) decrease. The hole depth can therefore also be related to the quantity of delivery for the given experimental conditions. Human abdominal skin and porcine skin from around the torso of the pig were used to obtain a wide range of Young’s moduli. The skin was injected with a jet with $u_0=159 (\pm 2)$ m/s, $D_0=152 \mu\text{m}$, and $x_s=1$ mm (submerged) ($n=4$).

and intramuscular injections [26]. A more accurate determination of the Young's modulus of skin such as multi-axial measurement may capture a more detailed role skin properties in jet injection [27].

4.3. Prediction of hole depth

Hole depth, h_d , in the skin clearly plays a major role in achieving a good injection. The depth of the hole not only influences the type of delivery (intra-dermal, subcutaneous, or intramuscular) but also the efficiency of delivery. Data in Fig. 8 reveal that as the hole depth decreases so does the percent delivery under the same experimental conditions.

Two mathematical models were developed to predict h_d in skin and polyacrylamide gels as a function of jet parameters and mechanical properties of the material. Such models may provide guidelines for the design of jet injectors and test the current understanding of jet penetration. The first model, the simpler of the two, predicts h_d in polyacrylamide gels and the second model predicts h_d in skin.

The predictive model for h_d presented in Eq. (6) relates the hole depth in polyacrylamide gels to the

initial conditions of the jet (velocity, nozzle diameter, and standoff distance) and σ_c . It was assumed that the failure of the gels in the direction of the jet was caused by compression, thereby σ_c could be independently measured as the critical stress for failure under compression (0.065 MPa, 0.104 MPa, 0.158 MPa, 0.230 MPa and 0.699 MPa for 10%, 15%, 20%, 25%, and 30% acrylamide gels, respectively).

Experimentally measured h_d in gels correlated with the predicted values ($r=0.94$, Fig. 9a). The range of hole depths in Fig. 9a was created by varying jet exit velocity (110–200 m/s), nozzle diameter (76–304.8 μm), standoff distance (1–5.8 mm), and gel's mechanical properties ($\sigma_c=0.065$ –0.699). The mean error between the predicted and the measured hole depths was 20%. The difference between the measured and predicted values might be due to additional modes of failure beyond compression, however, the hole depth was found to be independent of the critical shear stress (data not shown). Typically, holes created by the jet were cylindrical in shape and tapered at the end such as in Fig. 9b.

Compared to gels, predictions of h_d in skin are complicated by two factors: (i) the fluid dynamics

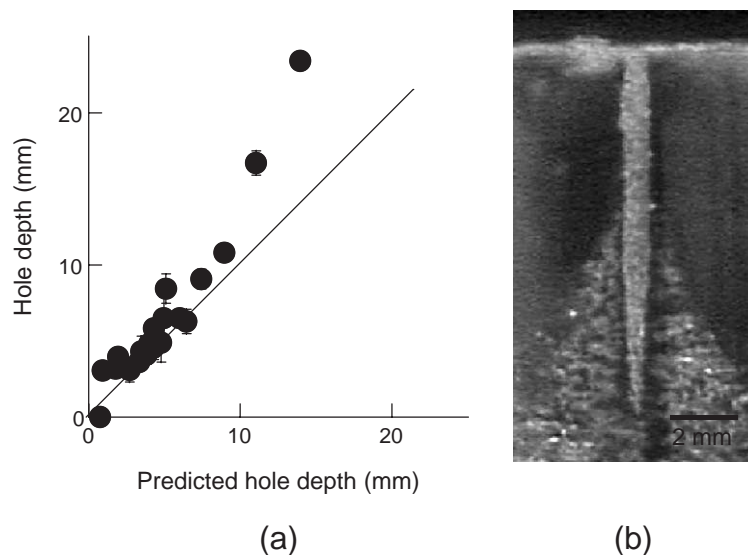


Fig. 9. (a) The predicted hole depths in polyacrylamide gels according to Eq. (6) correlated well ($r=0.94$) with the measured values overestimating the magnitude by an average of 20%. The velocity, nozzle diameter, standoff distance, and the critical stress for compressive failure were varied experimentally to test the modeled hole depth. For some of the experiments the water jet was ejected in air at a standoff distance of 1 mm above the gel. Since the surrounding air posed a low resistance to the water jet compared to ejecting into water (submerged), the standoff distance was assumed to be 0 when jets were ejected into air ($n=3$ –5). (b) A typical hole created in gel is cylindrical in shape and tapered at the terminal end. Polyacrylamide gels are clear allowing the hole to be visualized through the outer walls of the gel.

within the skin is more complicated than that in the gels due to backflow and (ii) σ_c for skin cannot be easily measured and was obtained by fitting Eq. (10) to experimentally measured h_d . Eq. (10), which relates h_d in skin to the initial jet parameters (u_0 and D_0) and σ_c , well described the experimental hole depths in the skin (Fig. 10). Human and porcine skin pieces of different mechanical properties were injected with jets with various exit velocities (120–200 m/s) and nozzle diameters (76–304.8 μm). Data for each skin sample are shown by a different symbol in Fig. 10. The correlation between the experimental data and the model should be assessed for each individual series of symbols rather than the collection of points since the critical stress was a fitted parameter (only one value of σ_c per set of symbols). For example, the series depicted by closed triangles has a correlation coefficient of 0.88 showing that the theory reasonably predicts the experiments. One major limitation of the model is that it does not predict a dependence of h_d on the standoff distance. This is due to the way in which the centerline velocity for the system was determined (Theory). Experimentally, hole depth decreases as the standoff distance is increased (Fig. 11) under submerged

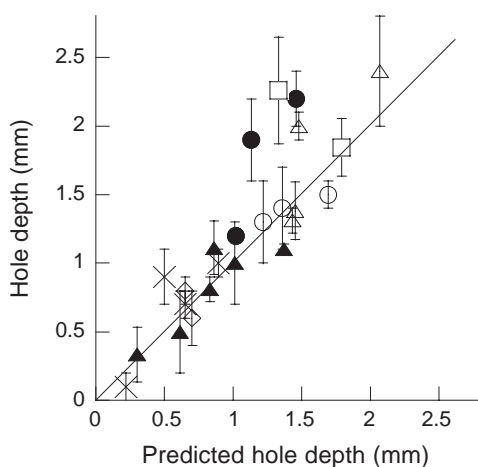


Fig. 10. Hole depths in human (\square , \triangle) and porcine skin (x , \blacktriangle , \circ , \diamond) created by jets of various conditions were compared with the predicted values based on Eq. (10) with σ_c as a fitted parameter. Each symbol represents a skin sample possessing different mechanical properties. Using the relationship of σ_c and E_{skin} in Fig. 12 together with Eq. (10), the hole depths created in a porcine skin sample (\bullet) were predicted with 31% error.

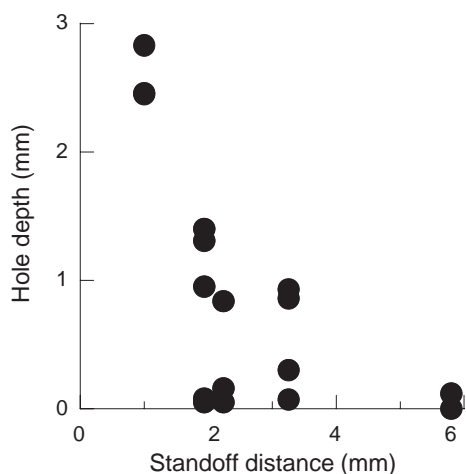


Fig. 11. Jet penetration is a function of the distance the nozzle is away from the skin, the standoff distance. Jets were ejected under submerged conditions with $u_0=154$ m/s and $D_0=152$ μm into human skin $E_{\text{skin}}=0.26$ MPa. Shallow hole depths were usually accompanied by a wide area of the epidermis that was disrupted.

conditions. The high variability present in Fig. 11 may have originated from the existence of a transition region for jets that has been previously reported [14].

To convert Eq. (10) into a predictive model, σ_c for skin was correlated to Young's modulus of skin (E_{skin}) since the latter can be measured experimentally. The critical stress increased from 0.46 to 5.80 MPa as the Young's modulus increased from 0.26 to 0.96 MPa (Fig. 12). Using this relation, a skin sample with $E_{\text{skin}}=0.50$ MPa possessed $\sigma_c=2.03$ MPa (Fig. 12). The hole depths predicted for this sample, by first predicting σ_c using data in Fig. 12 and then using Eq. (10), had a 31% mean error from the measured values (closed circles in Fig. 10). The range of critical stress derived from the model (0.46–5.8 MPa) is generally less than literature reports [19,28,29]. The Young's modulus of skin is highly dependent on the method of measurement. Therefore, the quantitative relationship between Young's modulus and critical stress should be used only when the Young's modulus is measured as described in Materials and methods.

The studies reported here provide an in-depth characterization and analysis of hole formation in the skin. The model described here to predict the hole depth in skin is the first major step in developing a predictive

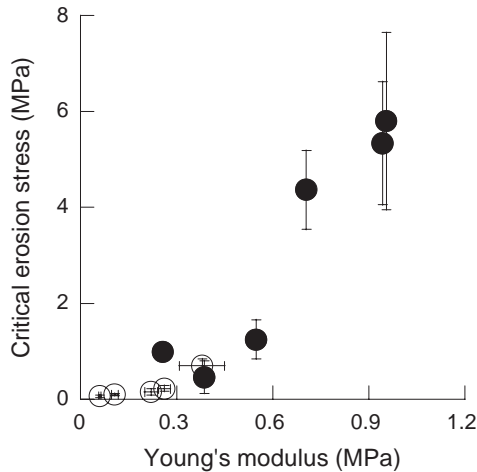


Fig. 12. The critical stress for jet impingement failure of the skin (●) was determined from experimental hole depths in conjunction with Eq. (10), the model for hole depth in skin. The critical stress is dependent on the Young's moduli of the human and porcine skin samples. From the relationship between the σ_c and E_{skin} future σ_c can be predicted based on a known value of E_{skin} and used in Eq. (10) to predict the hole depth. The critical stress of hole formation in polyacrylamide gels (○), which was independently measured, was a nonlinear function of the Young's modulus [6] ($n=3-5$).

model of drug delivery by jet injection. Further experimental and modeling work is required to model the dispersion of fluid into the skin in order to develop a complete model for drug delivery by jet injection. A model for drug delivery by jet injection would allow prediction of the quantity of drug delivered in addition to the type of injection (intra-dermal, subcutaneous, or intramuscular) and may aid in the development of new generations of jet injectors that avoid interactions with nerve endings suggested to be the primary source of pain associated with jet injections.

5. Conclusion

The hole depth created in skin by jet injection has been quantified and its dependence on jet properties and the uniaxial Young's modulus of skin has been determined. Coincident locations of L_m and the terminus of the hole have confirmed the hole formation–dispersion mechanism of jet injections. A model was developed to describe the hole depth in skin and polyacrylamide gels as functions of jet and material properties. A simplified model predicted the hole

depths in polyacrylamide gels with a 20% error. The model also described the hole depths in the skin. The critical stress for skin failure due to jet impingement in human and porcine skin was found to range from 0.46 to 5.8 MPa depending on the Young's modulus of skin.

Nomenclature

D_0	Nozzle diameter
u_0	Jet exit velocity
u_m	Jet centerline velocity
u_{mc}	Critical centerline velocity
x	Distance from the nozzle in the direction of flow
x_s	Standoff distance
α	Ratio of nozzle diameter to hole diameter
H	Hole diameter
h_d	Hole depth
L_m	Distance from the top of the skin to the maximum width of dispersion
E_{skin}	Young's modulus of skin
σ	Stress
ε	Strain
F	Force
A_{oc}	Original cross-sectional area
σ_c	Critical stress for jet impingement failure
ρ	Density of fluid [1000 kg/m^3]
C_2	Constant describing the spread of the jet, 0.081
x_0	Length of initial section of the jet
Q_{failure}	Rate of hole progression (material failure)
Q_{fluid}	Volumetric flow rate
m	Slope of u_m/u_0 vs. x/D_0
b	Constant

Acknowledgements

This work was supported by Materials Research Laboratory at University of California, Santa Barbara, CA, USA.

References

- [1] R.A. Hingson, H.S. Davis, M. Rosen, Historical development of jet injection and envisioned uses in mass immunization and mass therapy based upon 2 decades experience, *Military Medicine* 128 (1963) 516–524.

- [2] D.L.P.D. Bremseth, F.M.D. Pass, Delivery of insulin by jet injection: recent observations, *Diabetes Technology and Therapeutics* 3 (2001) 225–232.
- [3] P.A. Furth, A. Shamay, R.J. Wall, L. Hennighausen, Gene transfer into somatic tissue, *Analytical Biochemistry* 205 (1992) 365–368.
- [4] R.J. Mumper, Z. Cui, Genetic immunization by jet injection of targeted pDNA-coated nanoparticles, *Methods* 31 (2003) 255–262.
- [5] J.R. Schramm, S. Mitragotri, Transdermal drug delivery by jet injectors: energetics of jet formation and penetration, *Pharmaceutical Research* 19 (2002) 1673–1679.
- [6] J.R. Schramm-Baxter, J. Katrencik, S. Mitragotri, Jet injection into polyacrylamide gels: investigation of jet injection mechanics, *Journal of Biomechanics* 37 (2004) 1181–1188.
- [7] J.R. Schramm-Baxter, S. Mitragotri, Needle-free jet injections: dependence of jet penetration and dispersion in the skin on jet power, *Journal of Controlled Release* 97 (2004) 527–535.
- [8] N. Inoue, D. Kobayashi, M. Kimura, M. Toyama, I. Sugawara, S. Itoyama, M. Ogihara, K. Sugibayashi, Y. Morimoto, Fundamental investigation of a novel drug delivery system, a transdermal delivery system with jet injection, *International Journal of Pharmaceutics* 137 (1996) 75–84.
- [9] A.K. ElGeneidy, A.A. Bloom, J.H. Skerman, R.E. Stallard, Tissue reaction to jet injection, *Oral Surgery, Oral Medicine, and Oral Pathology* 38 (1974) 501–511.
- [10] D.A. Fletcher, D.V. Palanker, Pulsed liquid microjet for microsurgery, *Applied Physics Letters* 78 (2001) 1933–1935.
- [11] E.-A. Brujan, K. Nahen, P. Schmidt, A. Vogel, Dynamics of laser-induced cavitation bubbles near elastic boundaries: influence of the elastic modulus, *Journal of Fluid Mechanics* 433 (2001) 283–314.
- [12] A.W. Momber, R. Kovacevic, Test parameter analysis in abrasive water jet cutting of rocklike materials, *International Journal of Rock Mechanics* 34 (1997) 17–25.
- [13] J. Wang, D.M. Guo, A predictive depth of penetration model for abrasive waterjet cutting of polymer matrix composites, *Journal of Materials Processing Technology* 121 (2002) 390–394.
- [14] K.A. Mazurek, N. Rajaratnam, D.C. Sego, Scour of cohesive soil by submerged circular turbulent impinging jets, *Journal of Hydraulic Engineering* 127 (2001) 598–606.
- [15] O.O. Aderibigbe, N. Rajaratnam, Erosion of loose beds by submerged circular impinging vertical turbulent jets, *Journal of Hydraulic Research* 34 (1996) 19–33.
- [16] T.B. Frick, D.D. Marucci, J.A. Cartmill, C.J. Martin, W.R. Walsh, Resistance forces acting on suture needles, *Journal of Biomechanics* 34 (2001) 1335–1340.
- [17] B.P. Pereira, P.W. Lucas, T. Swee-Hin, Ranking the fracture toughness of thin mammalian soft tissues using the scissors cutting test, *Journal of Biomechanics* 30 (1997) 91–94.
- [18] S.P. Davis, B.J. Landis, Z.H. Adams, M.G. Allen, M.R. Prausnitz, Insertion of microneedles into skin: measurement and prediction of insertion force and needle fracture force, *Journal of Biomechanics* 37 (2004) 1155–1163.
- [19] J. Ankersen, A.E. Birkbeck, R.D. Thomson, P. Vanezis, Puncture resistance and tensile strength of skin stimulants, *Proceedings of the Institution of Mechanical Engineers. Part H, Journal of Engineering in Medicine* 213 (1999) 493–501.
- [20] N. Rajaratnam, Erosion by submerged circular jets, *Journal of the Hydraulics Division—ASCE* 108 (1982) 262–267.
- [21] G.N. Abramovich, *The Theory of Turbulent Jets*, The M.I.T. Press, Cambridge, MA, 1963.
- [22] M.L. Albertson, Y.B. Dai, R.A. Jensen, H. Rouse, Diffusion of submerged jets, *Transactions of the American Society of Civil Engineers* 115 (1950) 639–664.
- [23] N. Rajaratnam, *Turbulent Jets*, Elsevier, Amsterdam, 1976.
- [24] N. Rajaratnam, P.M. Steffler, S.A.H. Rizvi, P.R. Smy, An experimental study of very high velocity circular water jets in air, *Journal of Hydraulic Research* 32 (1994) 461–470.
- [25] F. Risso, J. Fabre, Diffusive turbulence in a confined jet experiment, *Journal of Fluid Mechanics* 337 (1997) 233–261.
- [26] S. Wagner, G. Dues, D. Sawitzky, P. Frey, B. Christ, Assessment of the biological performance of the needle-free injector INJEX using the isolated porcine forelimb, *British Journal of Dermatology* 150 (2004) 455–461.
- [27] S. Diridollou, F. Patat, F. Gens, L. Vaillant, D. Black, J.M. Lagarde, Y. Gall, M. Berson, In vivo model of mechanical properties of human skin under suction, *Skin Research and Technology* 6 (2000) 214–221.
- [28] R.H. Wildnauer, J.W. Bothwell, A.B. Douglass, Stratum corneum biomechanical properties: I. Influence of relative humidity on normal and extracted human stratum corneum, *Journal of Investigative Dermatology* 56 (1971) 72–78.
- [29] M. Kendall, S. Rishworth, F. Carter, T. Mitchell, Effects of relative humidity and ambient temperature on the ballistic delivery of micro particles to excised porcine skin, *Journal of Investigative Dermatology* 122 (2004) 739–746.